Plant Protection, 10 (02) 2026. 199-214 DOI:10.33804/pp.010.02.5827

Available Online at EScience Press

Plant Protection

ISSN: 2617-1287 (Online), 2617-1279 (Print)

http://esciencepress.net/journals/PP

Research Article

Synergistic Effects of Citrus Waste-Mediated Silver and Copper Nanoparticles on the Antioxidant Defense System of Kinnow in the Management of Citrus Canker

[a]Azeem Akram, [a]Muhammad Atiq, [a]Abdul Rehman, [b]Muhammad Sufyan

[a] *Department of Plant Pathology, University of Agriculture, Faisalabad, Pakistan.*
[b] *Department of Entomology, University of Agriculture, Faisalabad, Pakistan.*

ARTICLE INFO

Article history
Received: 4th September, 2025
Revised: 7th March, 2026
Accepted: 8th March, 2026

Keywords
Citrus reticulate
Xanthomonas citri subsp. citri
AgNPs
CuNPs
Antioxidant defense enzymes

ABSTRACT

This study investigated the synthesis and characterization of silver and copper nanoparticles derived from citrus peel extract and evaluated their synergistic effects on the antioxidant defense system of Kinnow for the management of citrus canker. UV-Vis spectroscopy confirmed nanoparticle formation with surface plasmon resonance peaks at 420 nm for AgNPs and 460 nm for CuNPs. Particle sizes ranged from 65-75 nm for AgNPs and 70-80 nm for CuNPs, with zeta potentials of -30 mV and -25 mV, respectively, indicating stable colloidal dispersions. X-ray diffraction analysis confirmed crystalline face-centered cubic structures, while FTIR analysis revealed that bioactive functional groups from citrus peel extract, including phenolics, flavonoids, and proteins, were involved in the reduction, capping, and stabilization of the nanoparticles. Scanning electron microscopy showed predominantly spherical morphologies with average sizes of 55 nm (AgNPs) and 65 nm (CuNPs). *In vitro* assays demonstrated that Ag-Cu hybrid nanoparticles exhibited the highest antibacterial activity against the citrus canker pathogen, producing an inhibition zone of 16.92 mm at 30 µg ml^{-1}, compared with AgNPs (14.48 mm) and CuNPs (11.52 mm). Greenhouse experiments showed that Ag-CuNPs significantly reduced disease incidence (16.23%), followed by AgNPs (18.91%) and CuNPs (27.97%). Field trials confirmed similar trends, with Ag-CuNPs recording the lowest disease incidence (19.33%). Antioxidant enzyme analyses indicated effective stress mitigation, as Ag-CuNP-treated plants exhibited reduced activities of SOD, POD, and CAT compared with other treatments. These findings highlight the potential of citrus waste-mediated nanoparticles as eco-friendly and sustainable tools for citrus canker management.

Corresponding Author: Muhammad Atiq
Email: muhammad.atiq@uaf.edu.pk
© 2026 EScience Press. All rights reserved.

Introduction

Citrus is a rich source of bioactive natural metabolites with substantial nutritional and medicinal value (Sengupta et al., 2024). However, this fruit crop is highly susceptible to a range of diseases (Irshad et al., 2012; Fateh et al., 2017; Saeed et al., 2019; Kalatippi et al., 2023), among which citrus canker, caused by *Xanthomonas citri* subsp. *citri* (*Xcc*), remains a persistent threat to the global citrus industry (Ali et al., 2023; Jamil et al., 2025). The disease is characterized by the formation of circular lesions (2-20 mm in diameter) on the abaxial surface of leaves. As infection progresses,

these lesions enlarge, become necrotic, and develop prominent water-soaked, oily margins. In advanced stages, chlorotic rings appear on fruits, leaves, and stems, leading to a rough and corky texture on the affected surfaces (Liu et al., 2021).

Currently, several management strategies for citrus canker are in practice, each with specific advantages and limitations (Tahir et al., 2023). Integrated disease management is generally employed, with the utilization of resistant cultivars considered an optimal approach. Nevertheless, even resistant cultivars may succumb under conducive environmental conditions, resulting in epidemic outbreaks of citrus canker (Atiq et al., 2022). Moreover, frequent use of copper-based products has led to the emergence of copper-resistant *Xcc* strains (Villamizar et al., 2020), while chemical residues pose risks to human health and the environment, emphasizing the need for eco-friendly alternatives (Fenta and Mekonnen, 2024).

In recent years, nanotechnology has emerged as a promising tool for plant disease management (Elmer and White, 2018; Hofmann et al., 2020; Shahbaz et al., 2023; Mehak et al., 2026). Nanoparticles (NPs) can be synthesized via physical or chemical methods; however, these conventional approaches often involve toxic chemicals, high energy consumption, large production costs, and limited biocompatibility (Menazea et al., 2020). To overcome these limitations, green synthesis of nanoparticles has gained attention due to its numerous advantages, including non-toxicity, sustainability, cost-effectiveness, scalability, reduced environmental hazard, functionalization potential, and the ability to produce diverse nanoparticle types (Nazir et al., 2019; Hano and Abbasi, 2021). Previous studies have demonstrated the biocidal potential of green-synthesized nanoparticles against citrus canker (Arif et al., 2022; Atiq et al., 2022).

Among various substrates for nanoparticle synthesis, citrus fruit waste, particularly peels, has proven to be a viable raw material owing to its abundance of bioactive compounds such as insoluble polysaccharides, polyphenols, soluble sugars, amino acids, pectin, ascorbic acid, and citric acid, which function as natural reducing and stabilizing agents during nanoparticle formation (Maqbool et al., 2023). The high moisture content of citrus peels (80-90% w/w) further facilitates the biosynthesis process (Khabeeri et al., 2020).

Nanoparticles have profound effects on plant physiology, biochemistry, and gene expression (Djanaguiraman et al., 2024; Hussain et al., 2026). Numerous studies have reported that nanoparticle application enhances plant growth and development by modulating nutrient availability and defense responses, and by directly interacting with plants under biotic stress (Dimkpa et al., 2017). Specifically, nanoparticles can regulate the activity of enzymatic antioxidants, which play a crucial role in converting reactive oxygen species, such as superoxides, into H_2O_2, thereby inhibiting pathogen progression (Sultana et al., 2021; Sharma et al., 2019). Such alterations in enzymatic metabolite levels may result from gene regulation or direct surface interactions between nanoparticles and antioxidant enzymes (Liu et al., 2020).

Based on these insights, the present study investigates the synergistic effects of citrus waste-mediated silver and copper nanoparticles on the regulation of antioxidant defense enzymes in kinnow, aiming to develop an effective strategy for the management of citrus canker.

Materials and Methods

Isolation, purification, and identification of the pathogen associated with citrus canker

The pathogen responsible for citrus canker was isolated from infected leaves following the method described by Ruangpan and Tendencia (2004). For purification, the bacterial culture was streaked onto fresh nutrient agar (NA) plates (9 cm diameter). For long-term preservation, the purified bacterial culture was mixed with 50% glycerol and stored in 1.5 ml Eppendorf tubes at -40°C (Model: DWVF1045CVT) to maintain viability (Hameed et al., 2021). Identification of the bacterium was conducted based on morphological characteristics, including colony color and shape, as well as biochemical tests such as Gram staining, KOH test, lecithinase test, catalase test, starch hydrolysis, and gelatin hydrolysis (Nauman et al., 2023).

Kinnow peel extract-mediated synthesis of AgNPs and CuNPs

Finely powdered Kinnow peels (10 g) were added to 450 ml of distilled water in a clean vessel. The mixture was tightly sealed with aluminum foil to prevent contamination and heated at 65°C for 15 min. After cooling to room temperature, it was centrifuged at 5,000 rpm for 15 min and then filtered through Whatman No. 1 filter paper. The resulting aqueous extract was stored at -4°C until further use.

For nanoparticle synthesis, 100 ml of 1 mM silver nitrate ($AgNO_3$) solution and 100 ml of 0.1 M anhydrous copper

sulfate ($CuSO_4$) solution were prepared separately. Fresh Kinnow peel extract (100 ml) was added dropwise to each precursor solution under continuous stirring. The pH of the silver mixture was adjusted to 8 using 0.1 M NaOH, while the copper mixture pH was adjusted to 4 using either 0.1 M NaOH or 0.05 M H_2SO_4. The silver reaction mixture was heated at 60°C for 15 min, and the copper reaction mixture at 70°C for 20 min. Both mixtures were then incubated at room temperature: 72 h for copper and 48-72 h for silver. The formation of a dark brown color in the silver solution and brown precipitates in the copper solution indicated successful synthesis of AgNPs and CuNPs, respectively.

Nanoparticles were collected by centrifugation at 5,000 rpm for 15 min, washed twice with double-distilled water to remove residual salts and unbound phytochemicals, and air-dried. The dried nanoparticles were stored in airtight containers (HLR105-GX) at room temperature to prevent contamination and degradation prior to application (Ghaffar et al., 2021). Hybrid nanoparticles (NPs) treatment was prepared by thoroughly mixing equal amounts of dried AgNPs and CuNPs powders, which were then suspended in distilled water at the desired concentration immediately before application.

Characterization of kinnow peel extract-based NPs

The successful synthesis of silver and copper nanoparticles was confirmed through various characterization techniques following the methodology of Hussain et al. (2019). UV-Visible spectroscopy (UV-1800) was used to monitor the reduction of metal ions and the stability of nanoparticles within the wavelength range of 300-700 nm. The particle size distribution and surface charge were determined using a Zeta analyzer (SZ-100V2). The crystalline nature and average particle size of the nanoparticles were analyzed by X-ray diffraction (XRD-6100). Furthermore, scanning electron microscopy (SEM, SU3500) was employed to examine the structural features and surface morphology of the synthesized nanoparticles.

In vitro* evaluation of kinnow peel extract-mediated NPs against *Xcc

This experiment was conducted twice following the methodology of Atiq et al. (2022) with slight modifications. Circular filter paper discs (1 cm diameter) were prepared and sterilized in an autoclave at 121°C and 15 psi for 15 min. A freshly grown culture of *Xcc* was uniformly spread over the surface of nutrient agar (NA) plates (9 cm diameter) using a sterile cotton swab inside a laminar airflow cabinet (RTVL-1312, Robus, United Kingdom).

Sterilized filter paper discs were immersed in different concentrations (10, 20, and 30 µg mL^{-1}) of Ag-Cu hybrid NPs, AgNPs, and CuNPs, and then placed at the center of the inoculated NA plates. Control plates received discs treated with sterile distilled water. The plates were sealed and incubated (Model IN-260) at 28 ± 2°C. The experiment was arranged in a completely randomized design (CRD) with three replicates per treatment.

The antibacterial activity was evaluated by measuring the inhibition zones formed around the treated discs. The diameter of the inhibition zones was recorded after 24, 48, and 72 h using a digital Vernier caliper (Model 500-196, Mitutoyo).

Assessment of kinnow peel extract-mediated NPs against citrus canker under greenhouse conditions

The greenhouse experiment was conducted twice following the protocol of Atiq et al. (2022) with minor modifications. One-year-old kinnow plants were selected due to their high susceptibility to infection and uniform growth characteristics, which facilitate reliable evaluation of nanoparticle treatments. The plants were obtained from the nursery of the Institute of Horticultural Sciences (IHS), University of Agriculture Faisalabad (UAF), Pakistan, and transplanted into pots (30 cm diameter) containing sterilized sandy clay soil to eliminate interference from pathogenic microorganisms.

Soil sterilization was performed by mixing the soil with 1% formalin solution, covering it with water-soaked gunny bags for three days to retain the fumes, and subsequently exposing it to open air for an additional 3-4 days to allow complete dissipation of formalin residues (Goswami et al., 2010).

To ensure uniform growth, the plants were pruned and regularly irrigated. Prior to inoculation, the plants were covered with polythene bags for 2 h under sunlight to create high humidity conditions and promote stomatal opening, thereby enhancing the likelihood of bacterial infection. The inoculum of *Xcc* was prepared at a concentration of 1×10^8 CFU ml^{-1} in sterile water and adjusted using a spectrophotometer (Hitachi U-2001, Model 121-003). The bacterial suspension was injected early in the morning into the midrib of kinnow leaves using a 1 cm^3 tuberculin syringe (Hameed et al., 2019).

Throughout the experiment, greenhouse conditions were maintained at approximately 80% relative humidity and a temperature range of 28-32°C using digital hygrometers (RS-325A) and thermometers (FT-85).

Three days after inoculation, nanoparticles (Ag-Cu hybrid NPs, AgNPs, and CuNPs) were applied at concentrations of 50, 75, and 100 mg L^{-1} using a hand sprayer (pressure: 0.25-0.45 MPa). The experiment was arranged in a completely randomized design with three replications, while tap water was sprayed on control plants.

Disease incidence was recorded at seven-day intervals for three consecutive observations and calculated using the formula (Iftikhar et al., 2024).

$$\text{DI (\%)} = \frac{\text{Number of Infected Plants}}{\text{Total Number of Plants Observed}} \times 100$$

Evaluation of kinnow peel extract-derived NP in the field for the management of citrus canker

A field trial was conducted twice following the method described by Atiq et al. (2022) with slight modifications. Approximately one-year-old kinnow plants, selected due to their high susceptibility to infection and uniform growth for experimental reliability, were obtained from the IHS nursery and transplanted into a plot of approximately 100 m^2 located in the Research Area of the Department of Plant Pathology, UAF. The plants were maintained at a spacing of 1.0 m between rows and 1.5 m between plants.

A 48-hr-old actively growing culture of *Xcc* was used to prepare an aqueous bacterial suspension, as this growth stage corresponds to the logarithmic phase, ensuring optimal bacterial density and pathogenicity. The bacterial concentration was adjusted to 1×10^8 CFU ml^{-1} using a spectrophotometer (Hitachi U-2001, model 121003UV/Vis).

Inoculation was performed in the early morning when stomatal openings are maximal. The *Xcc* suspension was injected into the midrib of kinnow leaves using a tuberculin syringe following the procedure described by Hameed et al. (2019). Three days after inoculation, nanoparticles, including Ag-Cu hybrid NPs (Ag-Cu NPs), AgNPs, and CuNPs, were applied at concentrations of 50, 75, and 100 mg L^{-1} using a hand sprayer operating at a pressure of 0.25-0.45 MPa. The experiment was arranged in a Randomized Complete Block Design (RCBD) with three replications per treatment. In the control treatment, plants were sprayed with tap water. Disease incidence was recorded at seven-day intervals for three observations. DI % was calculated using the formula described above.

Preparation of samples for biochemical analysis

Fresh leaf samples were collected from kinnow plants that had been inoculated and treated with green-synthesized nanoparticles, including kinnow peel-mediated AgNPs, CuNPs, and their hybrid formulation (Ag-Cu NPs) at concentrations of 50, 75, and 100 mg L^{-1}. Samples were also collected from inoculated but untreated plants, which served as controls.

Leaves were sampled from the upper, middle, and lower portions of plants maintained under greenhouse conditions in the Research Area of the Department of Plant Pathology, UAF. After collection, leaf tissues were cut into small pieces using sterilized scissors. Approximately 0.5 g of each sample was ground in a sterilized mortar and pestle using potassium phosphate buffer (pH 5.0). The homogenate was centrifuged (H-200 NR, Kokusan, Japan) at 12,000 rpm for 5 min, and the resulting supernatant was collected for subsequent biochemical analyses (Hameed et al., 2021).

Estimation of antioxidant enzyme activities in treated and untreated kinnow leaves

Catalase (CAT) activity was determined by mixing 100 µl of enzyme extract with 100 µl of 5.9 mM hydrogen peroxide, and the absorbance was measured at 240 nm. The results were expressed as µg g^{-1} fresh weight (FW).

For superoxide dismutase (SOD) estimation, the reaction mixture consisted of 100 µl enzyme extract, 100 µl nitroblue tetrazolium (NBT), 200 µl Triton X-500, 200 µl potassium phosphate buffer (pH 5.0), 200 µl methionine, and 800 µl distilled water. After adding 100 µl riboflavin, the mixture was exposed to UV light for 15 min. Absorbance was recorded at 560 nm, and SOD activity was expressed as µg g^{-1} FW.

Peroxidase (POD) activity was measured by mixing 800 µl potassium phosphate buffer (pH 5.0), 100 µl enzyme extract, 20 mM guaiacol, and 100 µl of 40 mM hydrogen peroxide. Absorbance was recorded at 470 nm, and enzyme activity was expressed as µg g^{-1} FW (Giannopolitis and Ries, 1977; Hameed et al., 2021).

Data analysis

Data obtained from laboratory and greenhouse experiments were analyzed using a Completely Randomized Design, whereas field experiments were analyzed using a Randomized Complete Block Design. Statistical analyses were performed using the PROC MIXED procedure in Statistical Analysis System (SAS), Version 9.4. When treatment effects were significant ($P \leq 0.05$), mean comparisons were conducted using Tukey's Honestly Significant Difference (HSD) test.

Results

Characterization of citrus peel extract-based NPs

Optical and surface characterization

UV-visible spectroscopy confirmed the successful synthesis of nanoparticles, as indicated by the characteristic surface plasmon resonance (SPR) peaks. AgNPs exhibited a distinct SPR peak at 420 nm with an optical density of 1.23 (Figure 1A), whereas CuNPs showed a peak at 460 nm with an optical density of 1.09 (Figure 1B).

Particle size distribution analysis revealed that AgNPs had a prominent peak at 70 nm, with a size range of 65-75 nm (Figure 1C). In contrast, CuNPs displayed a peak at 75 nm, within a size range of 70-80 nm (Figure 1D).

Zeta potential analysis indicated that both nanoparticle types possessed negative surface charges, suggesting good colloidal stability. AgNPs exhibited a peak zeta potential of -30 mV, with values ranging from -40 to -20 mV (Figure 1E), while CuNPs showed a peak zeta potential of -25 mV, with a range of -35 to -15 mV (Figure 1F).

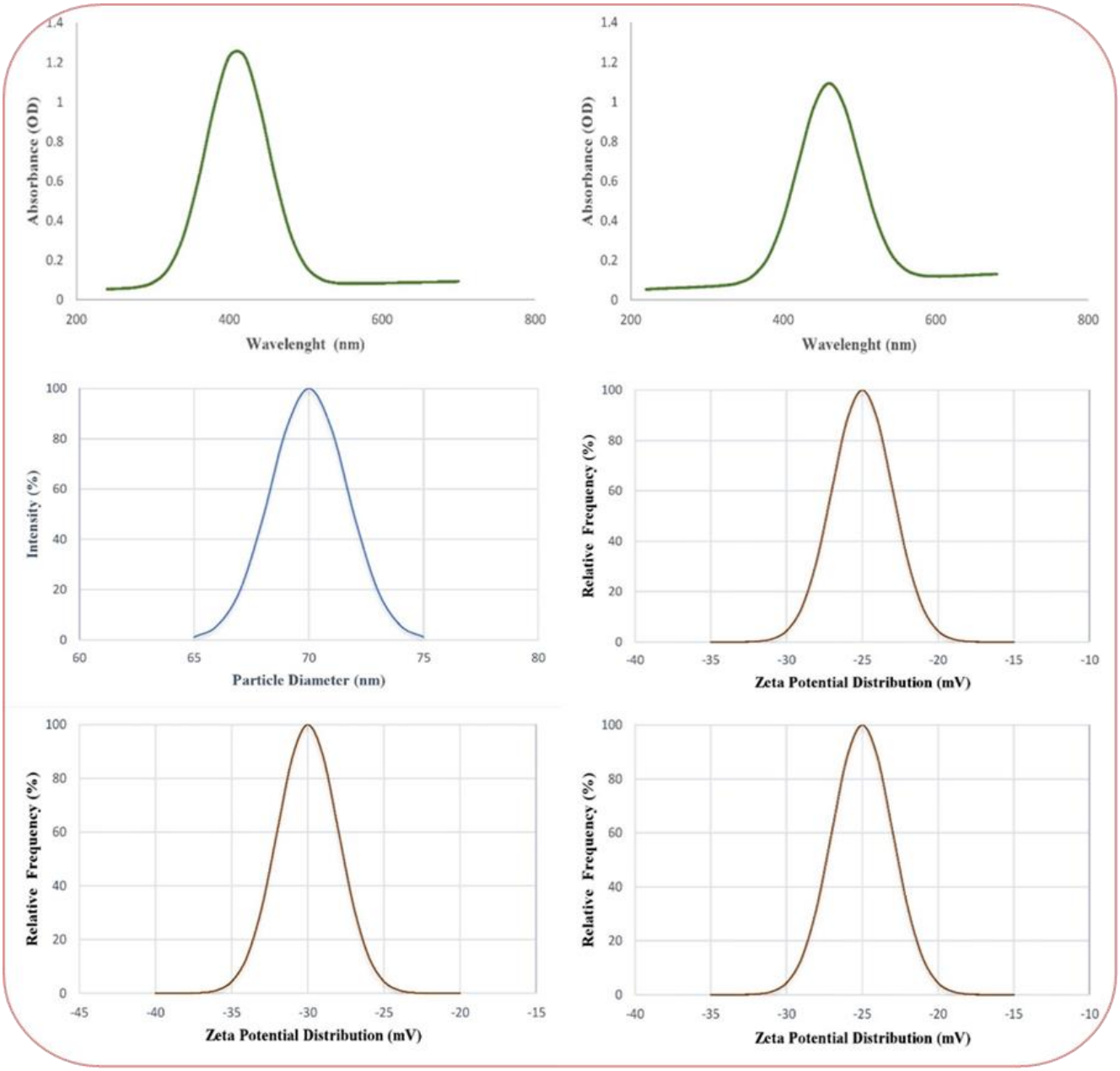


Figure 1. UV-Vis spectra (A, B), particle size distribution (C, D), and zeta potential analysis (E, F) of AgNPs and CuNPs, confirming their optical characteristics and surface charge properties.

Structural and morphological characterization

X-ray diffraction (XRD), Fourier-transform infrared (FTIR) spectroscopy, and scanning electron microscopy (SEM) were used to confirm the structural and morphological characteristics of the synthesized nanoparticles. XRD analysis verified the crystalline nature of both nanomaterials. AgNPs exhibited distinct diffraction peaks at 37.8°, 44.2°, 64.3°, and 77.2°, corresponding to the (111), (200), (220), and (311) lattice planes of the face-centered cubic (FCC) silver structure (Figure 2A). In contrast, CuNPs displayed peaks at 43.2°, 50.2°, and 74.1°, which were indexed to the (111), (200), and (220) planes of FCC copper (Figure 2B).

FTIR spectroscopy indicated the presence of bioactive functional groups originating from the plant extract, which likely participated in the reduction and stabilization of the nanoparticles. In AgNPs, absorption bands were observed at 3338 cm^{-1} (O–H/N–H stretching), 1630 cm^{-1} (C=O stretching, amide I), 1586 and 1383 cm^{-1} (C=C and N–H vibrations associated with flavonoid compounds), 1126 cm^{-1} (C–O stretching of polyols), and 757 cm^{-1} (C–H bending or Ag–O interactions) (Figure 2C). Similarly, CuNPs showed characteristic peaks at 3428 cm^{-1} (O–H/N–H stretching), 2930 cm^{-1} (C–H stretching), 1634 cm^{-1} (C=O stretching), 1381 cm^{-1} (C–H bending), and 1069 cm^{-1} (C–O stretching), suggesting the involvement of phenolics, flavonoids, and proteins in the formation and stabilization of the nanoparticles (Figure 2D). SEM analysis revealed that AgNPs possessed predominantly spherical morphology with particle sizes ranging from 50 to 60 nm, with an average diameter of approximately 55 nm (Figure 2E). In contrast, CuNPs appeared nearly spherical but showed the presence of larger clusters, representing agglomerates of primary particles, with sizes ranging from 60 to 70 nm and an average diameter of approximately 65 nm (Figure 2F).

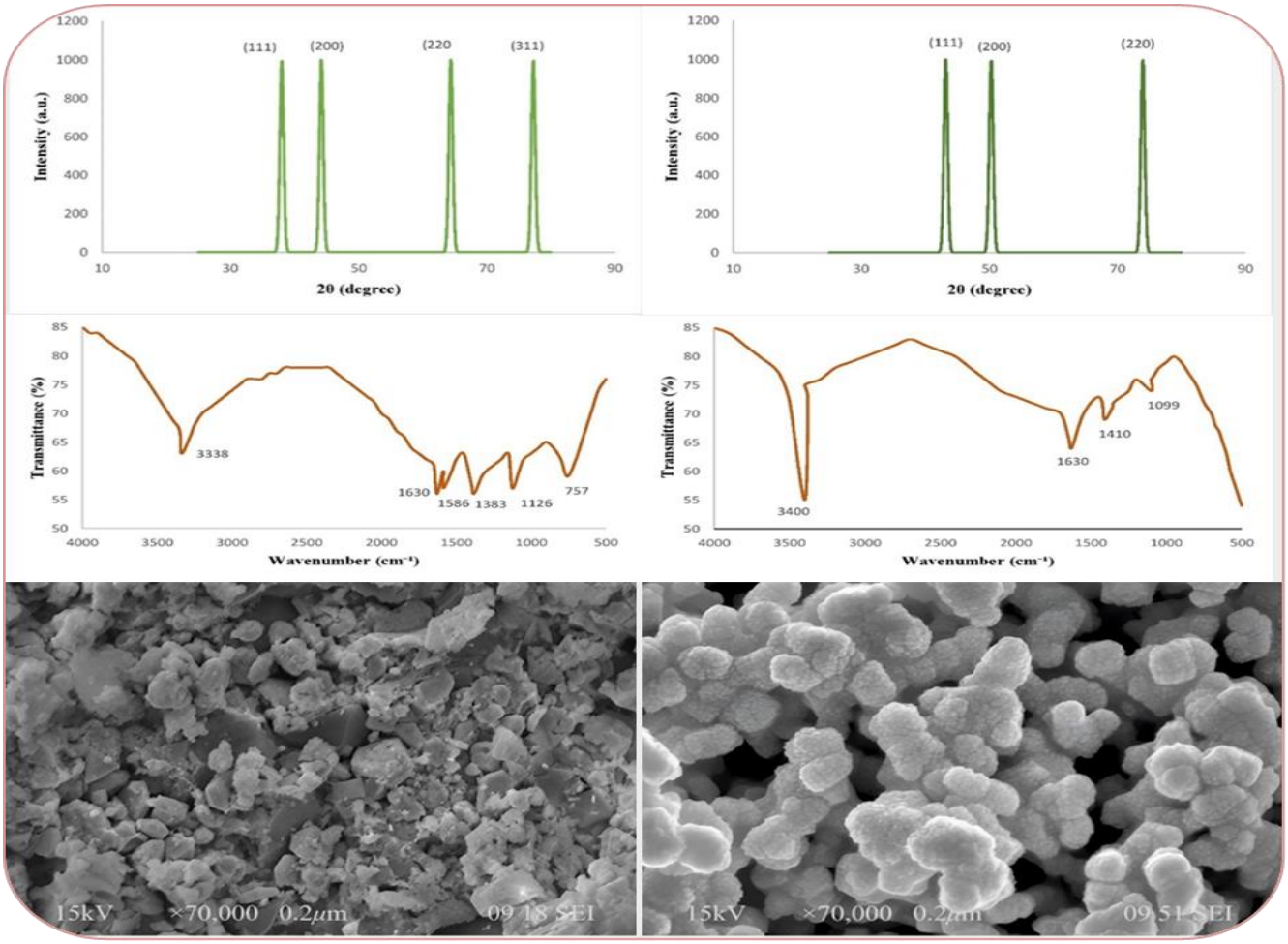


Figure 2. XRD patterns (A, B), FTIR spectra (C, D), and SEM images (E, F) of AgNPs and CuNPs confirming their crystalline structure, surface chemistry, and morphology.

Laboratory and greenhouse-scale investigation of citrus peel extract-based NPs against citrus canker

In the *in vitro* assay, Ag-Cu hybrid nanoparticles (Ag-CuNPs) produced the largest inhibition zone (14.331 mm), followed by AgNPs (11.846 mm) and CuNPs (8.633 mm), compared with the control treatment (Figure 3A). The interaction between treatment and concentration (T × C) indicated that Ag-CuNPs produced the greatest inhibition zones at 30 µg ml^{-1} (16.924 mm), 20 µg ml^{-1} (14.227 mm), and 10 µg ml^{-1} (11.843 mm). This was followed by AgNPs (9.333, 11.717, and 14.487 mm) and CuNPs (6.061, 8.314, and 11.524 mm) at concentrations of 10, 20, and 30 µg ml^{-1}, respectively, compared with the control (Figure 3B).

Similarly, the interaction between treatment and duration (T × D) showed that Ag-CuNPs exhibited the largest inhibition zones after 72 h (16.151 mm), followed by 48 h (14.514 mm) and 24 h (12.329 mm). In comparison, AgNPs produced inhibition zones of 13.713, 12.004, and 9.819 mm, while CuNPs produced 10.341, 8.524, and 7.034 mm at 72, 48, and 24 h, respectively, relative to the control treatment (Figure 3C).

In the greenhouse experiment, Ag-CuNPs resulted in the lowest disease incidence (16.229%), followed by AgNPs (18.909%) and CuNPs (27.966%), compared with the control treatment (Figure 3D). The interaction between treatment and concentration (T × C) revealed that the lowest disease incidence was observed with Ag-CuNPs (19.280%, 16.002%, and 13.403%), followed by AgNPs (21.891%, 19.058%, and 15.777%) and CuNPs (31.836%, 27.280%, and 24.781%) at concentrations of 50, 75, and 100 mg L^{-1}, respectively, compared with the control treatment (Figure 3E).

The interaction between treatment and duration (T × D) further demonstrated that Ag-CuNPs resulted in the lowest disease incidence (22.058%, 15.169%, and 11.459%), followed by AgNPs (25.724%, 18.669%, and 12.332%) and CuNPs (33.613%, 28.058%, and 22.226%) at 7, 14, and 21 days after treatment, respectively, compared with the control (Figure 3F).

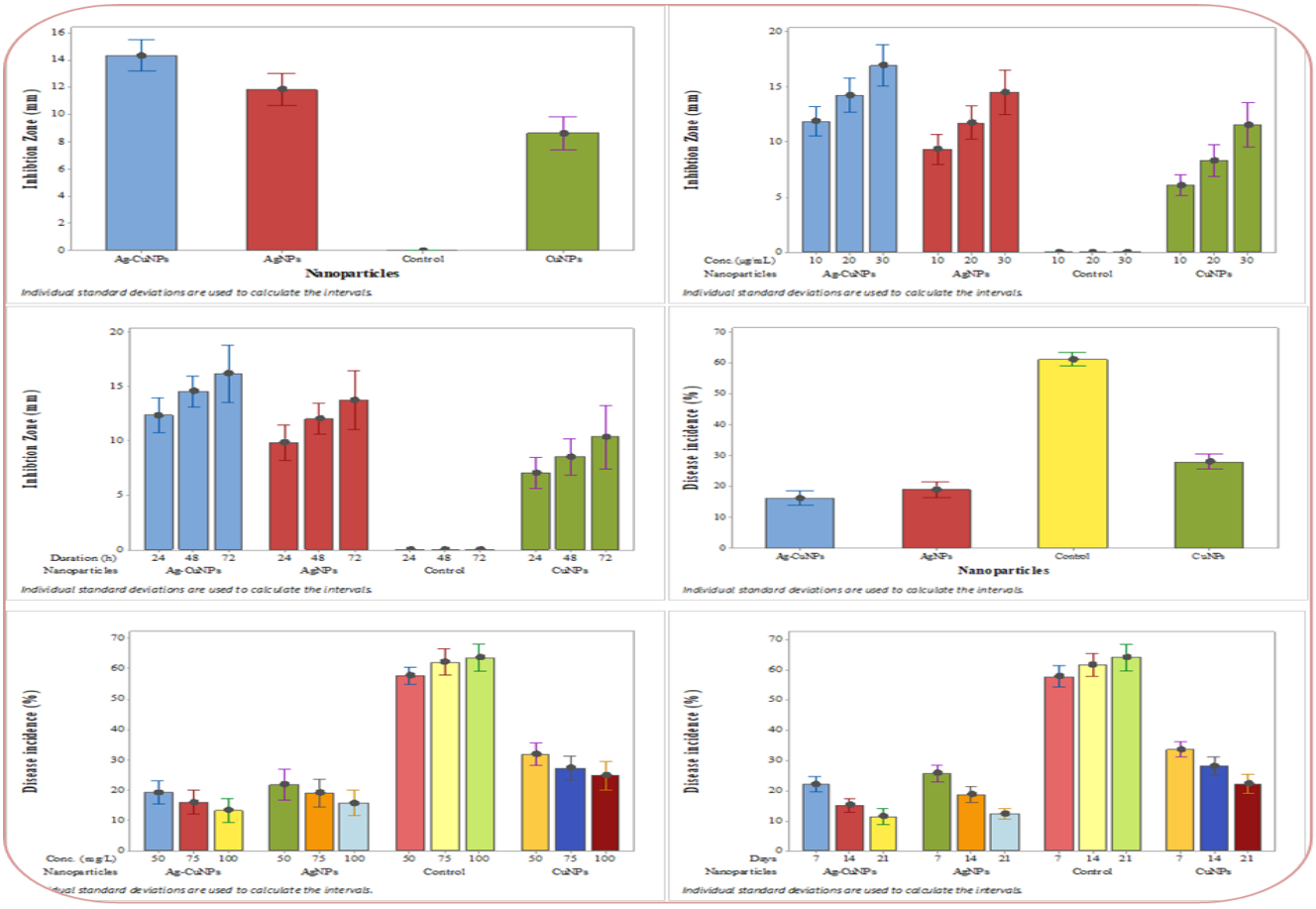


Figure 3. Effect of citrus peel extract-based nanoparticles on the incidence of citrus canker under laboratory (A-C) and greenhouse (D-F) conditions.

Field-scale management of citrus canker using citrus peel extract–based NPs and their impact on the antioxidant defense system of kinnow

Among the tested treatments, Ag-Cu hybrid nanoparticles (Ag-CuNPs) resulted in the lowest citrus canker incidence (19.339 %), followed by AgNPs (22.199 %) and CuNPs (30.116 %), compared with the control treatment (Figure 4A). The treatment × concentration (T×C) interaction indicated that the minimum disease incidence was recorded with Ag-CuNPs (22.390, 19.112, and 16.513 %), followed by AgNPs (25.181, 22.348, and 19.067 %) and CuNPs (33.986, 29.430, and 26.931 %) at concentrations of 50, 75, and 100 mg L^{-1}, respectively, compared with the control (Figure 4B).

Similarly, the treatment × duration (T×D) interaction revealed that the lowest disease incidence was observed with Ag-CuNPs (25.168, 18.279, and 14.569 %), followed by AgNPs (29.014, 21.959, and 15.622 %) and CuNPs (35.763, 30.208, and 24.376 %) at 7, 14, and 21 days after treatment, respectively, compared with the control (Figure 4C).

Biochemical analysis showed that Ag-CuNPs exhibited the lowest SOD activity (2.2833 µg g^{-1} FW), followed by AgNPs (3.4256 µg g^{-1} FW) and CuNPs (4.3878 µg g^{-1} FW), whereas the control treatment recorded the highest SOD activity (Figure 4D). The treatment × concentration interaction indicated that SOD activity increased progressively with increasing nanoparticle concentrations (50, 75, and 100 mg L^{-1}) within each treatment. At 50 mg L^{-1}, SOD activity was 2.1567, 3.0833, and 3.5733 µg g^{-1} FW for Ag-CuNPs, AgNPs, and CuNPs, respectively, all lower than that of the control. At 75 mg L^{-1}, SOD activity increased to 2.2567, 3.3900, and 4.4367 µg g^{-1} FW, respectively. Similarly, at 100 mg L^{-1}, SOD activity reached 2.4367, 3.8033, and 5.1533 µg g^{-1} FW for Ag-CuNPs, AgNPs, and CuNPs, respectively, but remained lower than the control (Figure 5).

Ag-Cu hybrid nanoparticles also exhibited the lowest POD activity (1.5911 µg g^{-1} FW), followed by AgNPs (3.5089 µg g^{-1} FW) and CuNPs (4.5711 µg g^{-1} FW), while the control treatment recorded the highest POD activity (Figure 4E). The T×C interaction demonstrated a gradual increase in POD activity with increasing concentrations (50, 75, and 100 mg L^{-1}) within each treatment. At 50 mg L^{-1}, POD activity was 1.4967, 3.2200, and 3.8833 µg g^{-1} FW for Ag-CuNPs, AgNPs, and CuNPs, respectively, all lower than the control. At 75 mg L^{-1}, POD activity increased to 1.5567, 3.4333, and 4.5933 µg g^{-1} FW, respectively. At 100 mg L^{-1}, POD activity further increased to 1.7200, 3.8733, and 5.2367 µg g^{-1} FW for Ag-CuNPs, AgNPs, and CuNPs, respectively, again indicating a concentration-dependent response (Figure 5).

Similarly, Ag-Cu hybrid nanoparticles exhibited the lowest CAT activity (1.7733 µg g^{-1} FW), followed by AgNPs (2.4711 µg g^{-1} FW) and CuNPs (4.0756 µg g^{-1} FW), whereas the control showed the highest CAT activity (Figure 4F). The T×C interaction revealed that CAT activity increased progressively with increasing nanoparticle concentrations (50, 75, and 100 mg L^{-1}). At 50 mg L^{-1}, CAT activity was 1.6867, 2.1133, and 3.4233 µg g^{-1} FW for Ag-CuNPs, AgNPs, and CuNPs, respectively, all lower than the control. At 75 mg L^{-1}, CAT activity increased to 1.7167, 2.4267, and 4.0433 µg g^{-1} FW, respectively. At 100 mg L^{-1}, CAT activity further increased to 1.9167, 2.8733, and 4.7600 µg g^{-1} FW, confirming consistent treatment × concentration interaction patterns (Figure 5).

Discussion

In recent years, increasing attention has been directed toward the beneficial utilization of fruit waste (Pechyen et al., 2021), as such materials are rich in diverse metabolites that can function as natural reducing and stabilizing agents during nanoparticle synthesis (Aswath et al., 2024). These plant-derived nanoparticles are considered promising alternatives to conventional chemical treatments because of their ease of synthesis, eco-friendly nature, and broad antimicrobial properties (Hayat and Afzaal, 2024).

In the present study, AgNPs and CuNPs were synthesized using Kinnow peel extract. Their formation was confirmed by UV-Visible spectroscopy, which showed characteristic surface plasmon resonance peaks. Similar observations have been reported by Ullah et al. (2019) and Asif et al. (2022). Particle size analysis revealed uniformly distributed nanoparticles with narrow size ranges, indicating controlled synthesis, which is consistent with the findings of Patra et al. (2015) and Manikandan and Sathiyabama (2015). Zeta potential analysis showed negative surface charges, suggesting good colloidal stability, in agreement with Michna et al. (2019) and Li et al. (2020). X-ray diffraction (XRD) analysis further confirmed the crystalline nature of both AgNPs and CuNPs, consistent with the structural characteristics reported by Nasab et al. (2020) and Nieto-Maldonado et al. (2022).

Fourier transform infrared (FTIR) analysis indicated the involvement of hydroxyl, amine, carbonyl, and flavonoid functional groups in the reduction and stabilization of nanoparticles, which is consistent with the findings of Ahsan et al. (2020) and Ullah et al. (2024). Scanning electron microscopy (SEM) revealed that AgNPs exhibited predominantly spherical morphology, whereas CuNPs appeared nearly spherical with the presence of larger clusters, likely representing agglomerates of primary particles. Similar observations have been reported by Babu Nagati et al. (2012) and Graves et al. (2016).

Among all treatments, Ag-Cu hybrid nanoparticles exhibited the largest inhibition zone at a concentration of 30 µg ml^{-1} after 24, 48, and 72 h under *in vitro* conditions, followed by AgNPs and CuNPs. To validate these results, the nanoparticles were further evaluated under greenhouse and field conditions. In both experiments, Ag-Cu hybrid nanoparticles applied at 100 mg L^{-1} resulted in the lowest disease incidence at 7, 14, and 21 days after treatment, followed by AgNPs and CuNPs.

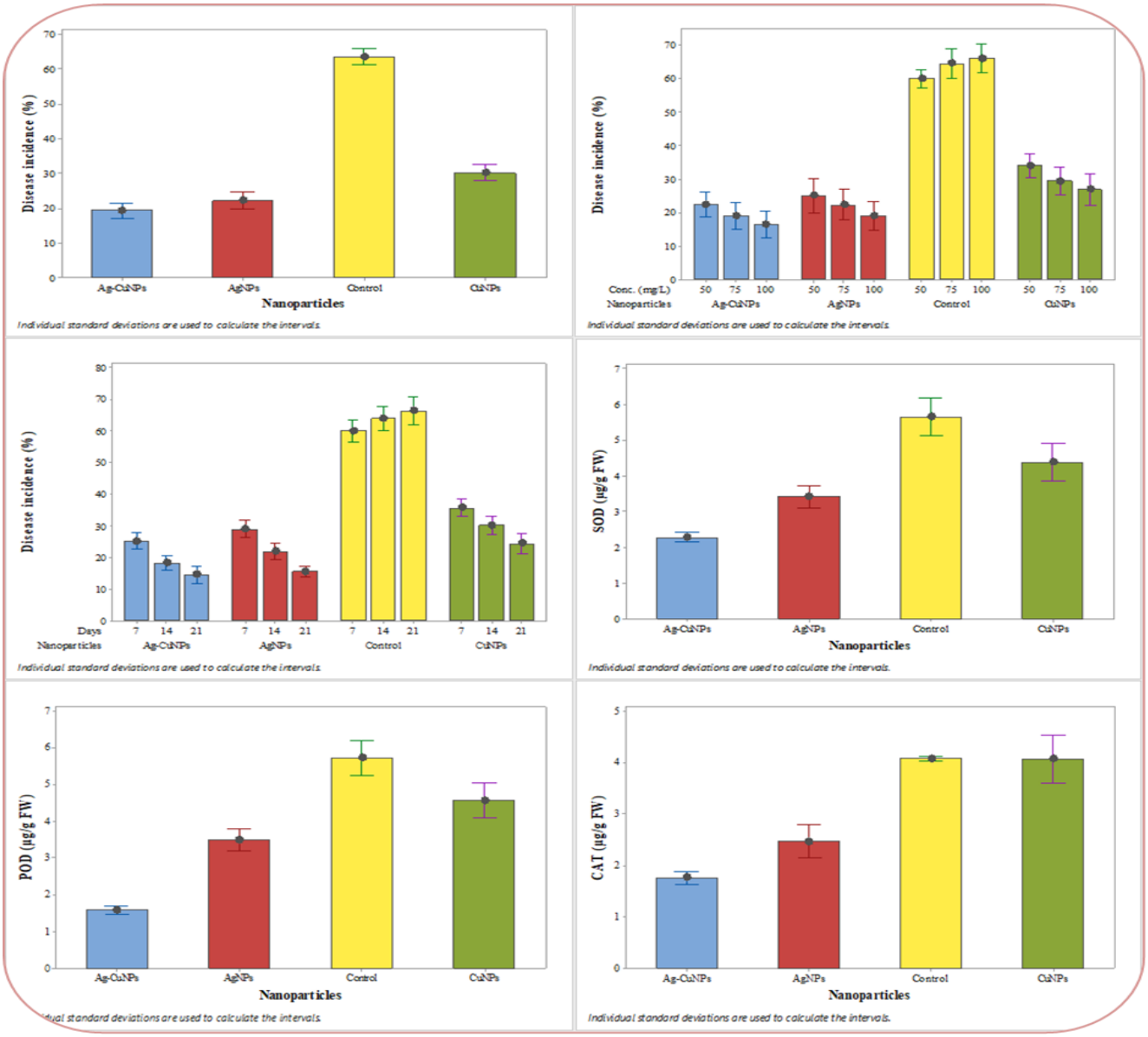


Figure 4. Field evaluation of citrus peel extract-based nanoparticles for the management of citrus canker and their effects on antioxidant enzyme activities. (A-C) Disease incidence under different nanoparticle treatments, concentrations, and time intervals. (D-F) Effects of nanoparticle treatments on antioxidant enzyme activities in kinnow leaves, including SOD, CAT, and POD.

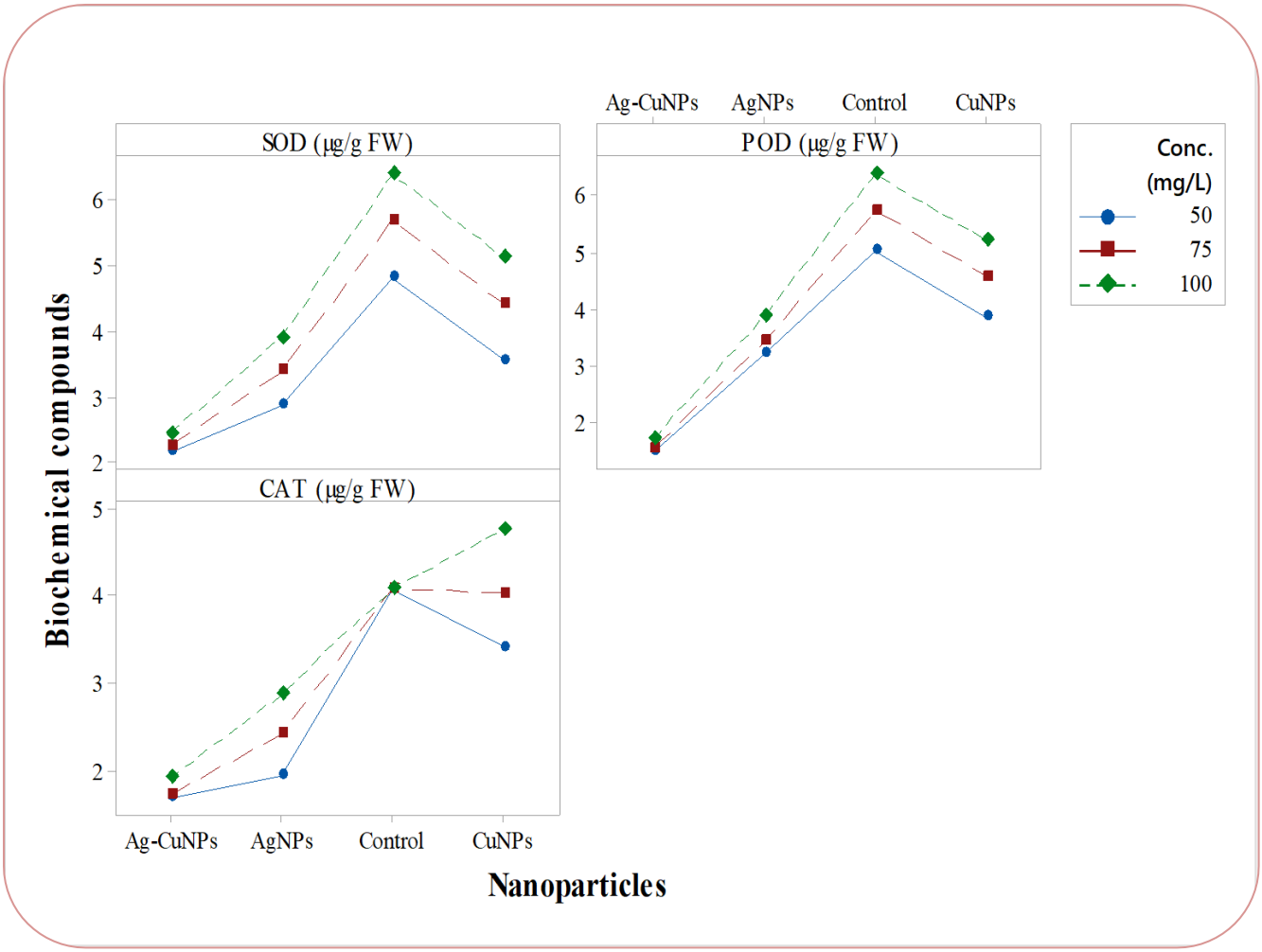


Figure 5. Concentration-dependent effects of citrus peel extract-derived nanoparticles on antioxidant enzyme activities (SOD, CAT and POD) in kinnow leaves.

The comparatively lower disease control observed under field conditions relative to greenhouse conditions may be attributed to environmental factors that promote nanoparticle leaching and reduce their stability and bioavailability. These conditions may limit the contact time of nanoparticles with the plant surface, reduce their uptake, and restrict their distribution within plant tissues, as reported by Liao et al. (2023).

Importantly, no visible phytotoxicity, growth abnormalities, or leaf chlorosis were observed in plants treated with 100 mg L^{-1} Ag-Cu hybrid nanoparticles in either greenhouse or field experiments. This finding indicates that the hybrid nanoparticle formulation is physiologically safe for plants, and its stability under experimental conditions was sufficient to maintain effective disease control.

These findings are consistent with previous studies reporting the antibacterial efficacy of metallic nanoparticles against several phytopathogenic bacteria, including *Xanthomonas citri* subsp. *citri* in citrus, *Clavibacter michiganensis* in tomato, *Ralstonia solanacearum* in eggplant, and *X. hortorum* in infected carrot seeds (Atiq et al., 2022; Attia et al., 2024; Hussain et al., 2024; Wohlmuth et al., 2024).

Silver nanoparticles exert antimicrobial activity by adhering to microbial cell surfaces, penetrating the cells, disrupting essential biomolecules, and generating reactive oxygen species (ROS) (Choi et al., 2010; Dakal et al., 2016; Abdalla et al., 2020) as illustrated in Figure 6. Copper nanoparticles, although sometimes less effective due to their relatively larger particle size, release Cu^{2+} ions that disrupt membrane integrity, interfere with enzymatic processes, and induce ROS-mediated cellular damage (Bayade et al., 2021) as shown in Figure 7.

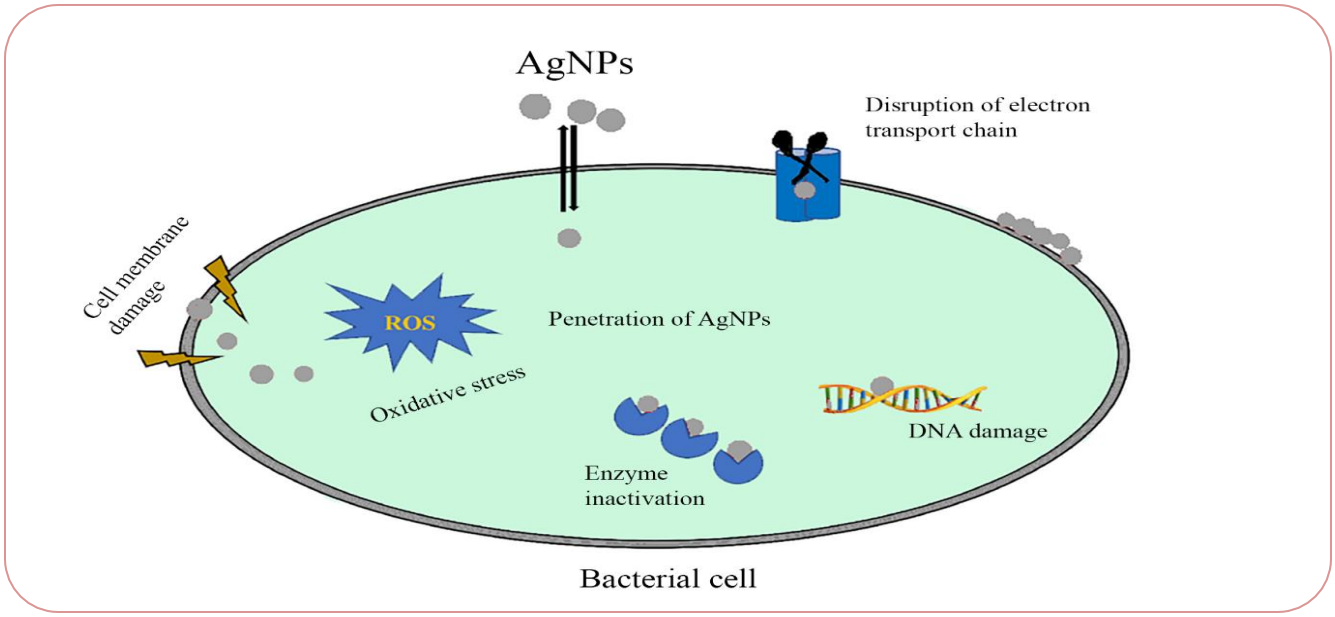


Figure 6. Generalized mode of action of silver nanoparticles illustrating their antimicrobial effects through surface interaction, cellular penetration, biomolecular disruption, and reactive oxygen species (ROS) generation.

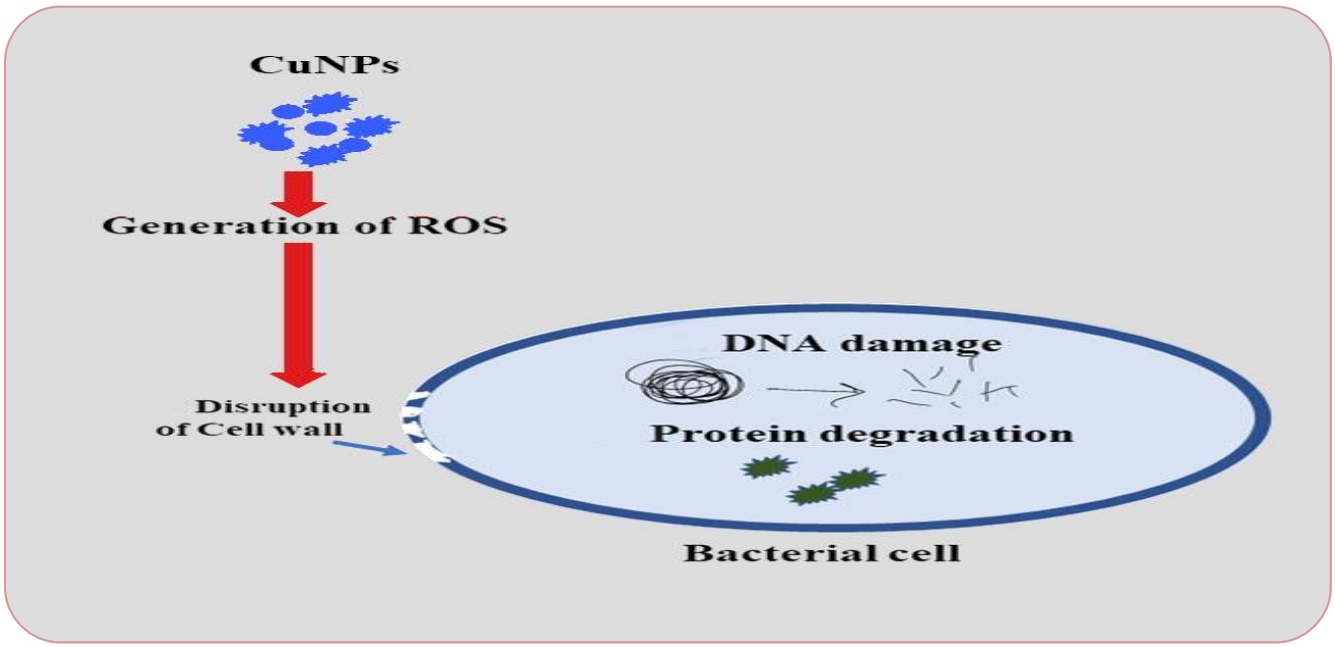


Figure 7. Proposed mode of action of copper nanoparticles illustrating antimicrobial effects via membrane disruption, protein interference, and ROS-mediated oxidative damage.

It is well established that nanoparticles can enhance plant defense mechanisms under biotic stress by modulating antioxidant production, reducing oxidative damage, and stabilizing cellular biochemical processes (Marslin et al., 2017; Quiterio-Gutiérrez et al., 2019; Ikram et al., 2022). In the present study, the effects of Kinnow peel extract-based AgNPs and CuNPs, applied individually and in combination, were evaluated for their role in regulating antioxidant defense responses in both treated and untreated Kinnow plants under biotic stress. Among all treatments, Ag-Cu hybrid nanoparticles resulted in the lowest levels of antioxidant enzymes (SOD, POD, and CAT), followed by AgNPs and CuNPs, compared with the control.

These findings are consistent with previous studies demonstrating that nanoparticles regulate plant biochemical responses under pathogen attack and alleviate oxidative damage. Similar observations have been reported in rice infected with *Magnaporthe oryzae* (Mazhar et al., 2023) and *Aspergillus flavus* (Sultana et al., 2021; Ejaz et al., 2023), citrus infected with *Candidatus Liberibacter asiaticus* (Umair Raza et al., 2023) and *X. citri* subsp. *citri* (Hussain et al., 2019), tomato infected with *Alternaria solani* (Narware et al., 2024), and wheat infected with *Puccinia striiformis* (Satti et al., 2022).

The elevated levels of SOD, POD, and CAT observed in inoculated untreated plants can be attributed to increased oxidative stress, likely associated with the accumulation of H_2O_2, which triggers enhanced antioxidant activity as part of the plant's defense response under pathogen attack (Biswas et al., 2020; Tarfeen et al., 2022). In contrast, the comparatively lower levels of SOD, POD, and CAT recorded in Ag-CuNP-treated grapefruit plants likely reflect the alleviation of *X. citri* subsp. *citri*-induced oxidative stress rather than suppression of the host defense system. This interpretation is supported by the concurrent reduction in disease incidence and the absence of phytotoxic effects, suggesting that the hybrid nanoparticles effectively mitigated oxidative damage and stabilized biochemical processes under biotic stress.

Conclusion

The combined application of silver and copper nanoparticles exerted a synergistic effect, resulting in maximum inhibition of *Xanthomonas citri* subsp. *citri* growth under laboratory conditions. Moreover, the combined use of AgNPs and CuNPs significantly enhanced disease suppression under both greenhouse and field conditions. This was accompanied by a marked downregulation of antioxidant enzyme activities in Kinnow plants, reflecting reduced pathogen-induced oxidative stress. Future research should focus on evaluating citrus peel-derived silver and copper nanoparticles against a broader spectrum of plant pathogens to further explore their potential for sustainable crop protection.

Acknowledgements

The authors are highly thankful to the Molecular Plant Bacteriology Laboratory, University of Agriculture, Faisalabad, Pakistan, for providing the research facilities.

Author's contributions

AA conducted the experiments, performed the data analysis, and prepared the initial draft of the manuscript. MA conceived and supervised the research project, guided the experimental design, and critically reviewed and revised the manuscript for intellectual content. AR and MS critically evaluated the study, contributed to editing and refining the manuscript, and assisted in improving the scientific clarity and overall presentation of the work. All authors read and approved the final version of the manuscript.

Research Funding

This research did not receive any grant from funding agencies.

Conflict of Interest

The authors declare no conflict of interest.

Sustainable Development Goals Targeted

SDG 2: Zero Hunger
SDG 9: Industry, Innovation, and Infrastructure
SDG 12: Responsible Consumption and Production

References

Abdalla, S.S.I., Katas, H., Chan, J.Y., Ganasan, P., Azmi, F., Busra, M.F.M., 2020. Antimicrobial activity of multifaceted lactoferrin or graphene oxide functionalized silver nanocomposites biosynthesized using mushroom waste and chitosan. RSC Advances 10, 4969-4983.

Ahsan, A., Farooq, M.A., Bajwa, A.A., Parveen, A., 2020. Green synthesis of silver nanoparticles using *Parthenium hysterophorus*: optimization, characterization and *in vitro* therapeutic evaluation. Molecules 25, 3324.

Ali, S., Hameed, A., Muhae-Ud-Din, G., Ikhlaq, M., Ashfaq, M., Atiq, M., Ali, F., Zia, Z.U., Naqvi, S.A.H., Wang, Y., 2023. Citrus canker: a persistent threat to the worldwide citrus industry-an analysis. Agronomy 13, 1112.

Arif, M., Ullah, R., Ahmad, M., Ali, A., Ullah, Z., Ali, M., Sher, H., 2022. Green synthesis of silver nanoparticles using *Euphorbia wallichii* leaf extract: Its antibacterial action against citrus canker causal agent and antioxidant potential. Molecules 27, 3525.

Asif, M., Yasmin, R., Asif, R., Ambreen, A., Mustafa, M., Umbreen, S., 2022. Green synthesis of silver

nanoparticles (AgNPs), structural characterization, and their antibacterial potential. Dose-Response 20, 15593258221088709.

Aswath, Y., Mubeen, M., Shakeel, O., Lalarukh, I., Ali, A., Aasim, M., Zeshan, M.A., Zulfiqar, T., Alhag, S.K., Al-Shuraym, L.A., 2024. Spatial distribution and molecular characterization of Huanglongbing and its vector in various citrus cultivars. Pakistan Journal of Agricultural Sciences 61, 266-279.

Atiq, M., Mazhar, H., Rajput, N.A., Ahmad, U., Hameed, A., Lodhi, A., 2022. Green synthesis of silver and copper nanoparticles from leaves of Eucalyptus globulus and assessment of its antibacterial potential towards *Xanthomonas citri* subsp. *citri* causing citrus canker. Applied Ecology and Environmental Research 20, 2205-2213.

Attia, M.S., Salem, S.S., Elakraa, A.A., Abdel-Maksoud, M.A., Malik, A., Kiani, B.H., Malash, M.N., El-Sayyad, G.S., 2024. Promising antagonistic effect of bimetallic silver-selenium nanoparticles against *Ralstonia solanacearum*-causing wilt disease in eggplant (*Solanum melongena* L.). Physiological and Molecular Plant Pathology 133, 102369.

Babu Nagati, V., Koyyati, R., Donda, M.R., Alwala, J., Kundle, K.R., Padigya, P.R.M., 2012. Green synthesis and characterization of silver nanoparticles from *Cajanus cajan* leaf extract and its antibacterial activity. International Journal of Nanomaterials and Biostructures 2, 39-43.

Bayade, G., Wu, M.R., Massicotte, R., Deryabin, D.G.E., Yahia, L.H., 2021. Biocidal properties of copper nanoparticles. Engineering of Biomaterials 24, 1-16.

Biswas, K., Adhikari, S., Tarafdar, A., Kumar, R., Saha, S., Ghosh, P., 2020. Reactive oxygen species and antioxidant defence systems in plants: Role and crosstalk under biotic stress. Sustainable Agriculture in the Era of Climate Change 9, 265-292.

Choi, O., Yu, C.P., Esteban, G.F., Hu, Z., 2010. Interactions of nanosilver with *Escherichia coli* cells in planktonic and biofilm cultures. Water Research 44, 6095-6103.

Dakal, T.C., Kumar, A., Majumdar, R.S., Yadav, V., 2016. Mechanistic basis of antimicrobial actions of silver nanoparticles. Frontiers in Microbiology 7, 1831.

Dimkpa, C.O., Bindraban, P.S., Fugice, J., Agyin-Birikorang, S., Singh, U., Hellums, D., 2017. Composite micronutrient nanoparticles and salts decrease drought stress in soybean. Agronomy for Sustainable Development 37, 5.

Djanaguiraman, M., Anbazhagan, V., Dhankher, O.P., Prasad, P.V., 2024. Uptake, translocation, toxicity, and impact of nanoparticles on plant physiological processes. Plants 13, 3137.

Elmer, W., White, J.C., 2018. The future of nanotechnology in plant pathology. Annual Review of Phytopathology 56, 111-133.

Fateh, F.S., Mukhtar, T., Kazmi, M.R., Abbassi, N.A., Arif, A.M., 2017. Prevalence of citrus decline in district Sargodha. Pakistan Journal of Agricultural Sciences 54, 9-13.

Fenta, L., Mekonnen, H., 2024. Microbial biofungicides as a substitute for chemical fungicides in the control of phytopathogens: current perspectives, and research directions. Scientifica 2024, 5322696.

Ghaffar, A., Kiran, S., Rafique, M.A., Iqbal, S., Nosheen, S., Hou, Y., Aimun, U., 2021. *Citrus paradisi* fruit peel extract mediated green synthesis of copper nanoparticles for remediation of Disperse Yellow 125 dye. Desalination and Water Treatment 212, 368-375.

Giannopolitis, C.N., Ries, S.K., 1977. Superoxide dismutases: I. Occurrence in higher plants. Plant Physiology 59, 309-314.

Goswami, R.S., Waldron, L., Machado, J., Cervigne, N.K., Xu, W., Reis, P.P., Bailey, D.J., Jurisica, I., Crump, M.R., Kamel-Reid, S., 2010. Optimization and analysis of a quantitative real-time PCR-based technique to determine microRNA expression in formalin-fixed paraffin-embedded samples. Biotechnology 10, 1-12.

Graves, J.E., Sugden, M., Litchfield, R.E., Hutt, D.A., Mason, T.J., Cobley, A.J., 2016. Ultrasound assisted dispersal of a copper nanopowder for electroless copper activation. Ultrasonics Sonochemistry 29, 428-438.

Hameed, A., Atiq, M., Javed, N., Ahmad, A., Ahmed, Z., 2019. Progressive alterations in mineral profiling of citrus infected with canker caused by *Xanthomonas axonopodis* pv. *citri* (Hasse). Applied Ecology and Environmental Research 17, 13625-13642.

Hameed, A., Atiq, M., Sahi, S.T., Rajput, N.A., Ahmed, Z., Alam, M.W., Alsamadany, H., Alzahrani, Y., Sarfraz, S., Altaf, J., Awan, S.A., 2021. Biochemical base of resistance in citrus against canker disease. Pakistan Journal of Agricultural Sciences 58, 1850-1858.

Hano, C., Abbasi, B.H., 2021. Plant-based green synthesis of nanoparticles: Production, characterization, and

applications. Biomolecules 12(1), 31.

Hayat, A., Afzaal, S., 2024. Copper nanoparticles (CuNPs) from citrus (kinnow) waste and their antibacterial action against canker-causing *Xanthomonas citri*. Journal of Hygienic Engineering and Design 48, 15-29.

Hofmann, T., Lowry, G.V., Ghoshal, S., Tufenkji, N., Brambilla, D., Dutcher, J.R., Wilkinson, K.J., 2020. Technology readiness and overcoming barriers to sustainably implement nanotechnology-enabled plant agriculture. Nature Food 1, 416-425.

Hussain, M., Raja, N.I., Mashwani, Z.U.R., Iqbal, M., Ejaz, M., Aslam, S., 2019. Green synthesis and evaluation of silver nanoparticles for antimicrobial and biochemical profiling in Kinnow (*Citrus reticulata* L.) to enhance fruit quality and productivity under biotic stress. IET Nanobiotechnology 13, 250-256.

Hussain, M.A., Nijabat, A., Rehman, M.M.U., Qurashi, R., Siddiqui, M.H., Alamri, S., Mashwani, Z.U.R., Leghari, S.U.K., Shah, M.A., Zaman, Q.U., 2024. Management of tomato bacterial canker disease by the green fabricated silver nanoparticles. BMC Plant Biology 24, 597.

Hussain, S., Younas, Z., Abasi, F., Nazik, M., Ahmad, F., Raja, N.I., Mukhtar, T., Manzoor, Z., Khan, R., Mashwani, Z.U.R., 2026. Deciphering the potential of silver-selenium nanocomposites on growth metrics, physiological attributes, and antioxidant profiles in cotton (*Gossypium hirsutum* L.). Plant Nano Biology 16, 100271. https://doi.org/10.1016/j.plana.2026.100271

Iftikhar, Y., Mubeen, M., Shakeel, O., Lalarukh, I., Ali, A., Aasim, M., Zeshan, M.A., Zulfiqar, T., Alhag, S.K., Al-Shuraym, L.A., 2024. Spatial distribution and molecular characterization of Huanglongbing and its vector in various citrus cultivars. Pakistan Journal of Agricultural Sciences 61, 266-279.

Ijaz, I., Gilani, E., Nazir, A., Bukhari, A., 2020. Detailed review on chemical, physical, and green synthesis, classification, characterizations, and applications of nanoparticles. Green Chemistry Letters and Reviews 13, 223-245.

Ikram, M., Raja, N.I., Mashwani, Z.U.R., Omar, A.A., Mohamed, A.H., Satti, S.H., Zohra, E., 2022. Phytogenic selenium nanoparticles elicited the physiological, biochemical, and antioxidant defense system amelioration of Huanglongbing-infected 'Kinnow' mandarin plants. Nanomaterials 12, 356.

Irshad, U., Mukhtar, T., Ashfaq, M., Kayani, M.Z., Kayani, S.B., Hanif, M., Aslam, S., 2012. Pathogenicity of citrus nematode (*Tylenchulus semipenetrans*) on *Citrus jambhiri*. Journal of Animal and Plant Sciences 22, 1014-1018.

Jamil, Z., Mukhtar, T., Raja, M.U., Shahbaz, M., Seelan, J.S.S., Tatar, M., Ali, A., Fatima, N., Bejaoui, R., Usanmaz Bozhüyük, A., 2025. Utilization of phytogenic silver nanoparticles and bacterial agents for the management of citrus canker disease. Turkish Journal of Agriculture and Forestry 49, 998-1008.

Kalatippi, A.S., Pandey, S.K., Huchche, A.D., Nair, R., 2023. Delayed harvesting and creasing fruit disorder in Nagpur mandarin (*Citrus reticulata* Blanco): Nature and alleviation through GA3 application. The Pharma Innovation Journal 12, 2308-2310.

Khabeeri, O.M., Al-Thabaiti, S.A., Khan, Z., 2020. *Citrus sinensis* peel waste assisted synthesis of AgNPs: effect of surfactant on the nucleation and morphology. SN Applied Sciences 2, 2038.

Li, W., Wei, W., Wu, X., Zhao, Y., Dai, H., 2020. The antibacterial and antibiofilm activities of mesoporous hollow Fe3O4 nanoparticles in an alternating magnetic field. Biomaterials Science 8, 4492-4507.

Liao, Y.Y., Pereira, J., Huang, Z., Fan, Q., Santra, S., White, J.C., Paret, M.L., 2023. Potential of novel magnesium nanomaterials to manage bacterial spot disease of tomato in greenhouse and field conditions. Plants 12, 1832.

Liu, W., Worms, I., Slaveykova, V.I., 2020. Interaction of silver nanoparticles with antioxidant enzymes. Environmental Science: Nano 7, 1507-1517.

Liu, Y., Benohoud, M., Yamdeu, J.H.G., Gong, Y.Y., Orfila, C., 2021. Green extraction of polyphenols from citrus peel by-products and their antifungal activity against *Aspergillus flavus*. Food Chemistry: X 12, 100144.

Manikandan, A., Sathiyabama, M., 2015. Green synthesis of copper-chitosan nanoparticles and study of its antibacterial activity. Journal of Nanomedicine and Nanotechnology 6, 1-18.

Maqbool, Z., Khalid, W., Atiq, H.T., Koraqi, H., Javaid, Z., Alhag, S.K., Al-Farga, A., 2023. Citrus waste as source of bioactive compounds: Extraction and utilization in health and food industry. Molecules 28, 1636.

Marslin, G., Sheeba, C.J., Franklin, G., 2017. Nanoparticles alter secondary metabolism in plants via ROS

burst. Frontiers in Plant Science 8, 832.

Mazhar, M.W., Ishtiaq, M., Maqbool, M., Hussain, S.A., 2023. Foliar application of zinc oxide nanoparticles improves rice yield under biotic stress posed by *Magnaporthe oryzae*. Archives of Phytopathology and Plant Protection 56, 1093-1111.

Mehak, A., Akram, A., Ali, A., Raja, N.I., Mukhtar, T., Seelan, J.S.S., Shahbaz, M., 2026. Nano-TiO_2 as a sustainable strategy to control root-knot nematodes (RKNs) in tomato (*Solanum lycopersicum* L.). Physiological and Molecular Plant Pathology 103122.

Menazea, A.A., 2020. Femtosecond laser ablation-assisted synthesis of silver nanoparticles in organic and inorganic liquids medium and their antibacterial efficiency. Radiation Physics and Chemistry 168, 108616.

Michna, A., Morga, M., Adamczyk, Z., Kubiak, K., 2019. Monolayers of silver nanoparticles obtained by green synthesis on macrocation modified substrates. Materials Chemistry and Physics 227, 224–235.

Narware, J., Singh, S.P., Ranjan, P., Behera, L., Das, P., Manzar, N., Kashyap, A.S., 2024. Enhancing tomato growth and early blight disease resistance through green-synthesized silver nanoparticles: Insights into plant physiology. South African Journal of Botany 166, 676-689.

Nasab, N.K., Sabouri, Z., Ghazal, M., Darroudi, M., 2020. Green-based synthesis of mixed-phase silver nanoparticles as an effective photocatalyst and investigation of their antibacterial properties. Journal of Molecular Structure 1203, 127411.

Nauman, M.D., Mushtaq, S., Khan, M.F., Ali, A., Naqvi, S.A.H., Haq, Z., Umar, U.U.D., 2023. Morphological, biochemical, and molecular characterization of *Xanthomonas citri* subsp. *citri* cause of citrus canker disease in Pakistan. Pakistan Journal of Botany 55, 2409-2421.

Nazir, K., Mukhtar, T., Javed, H., 2019. *In vitro* effectiveness of silver nanoparticles against root-knot nematode (*Meloidogyne incognita*). Pakistan Journal of Zoology 51, 2077-2083.

Nieto-Maldonado, A., Bustos-Guadarrama, S., Espinoza-Gomez, H., Flores-López, L.Z., Ramirez-Acosta, K., Alonso-Nuñez, G., Cadena-Nava, R.D., 2022. Green synthesis of copper nanoparticles using different plant extracts and their antibacterial activity. Journal of Environmental Chemical Engineering 10, 107130.

Patra, S., Mukherjee, S., Barui, A.K., Ganguly, A., Sreedhar, B., Patra, C.R., 2015. Green synthesis, characterization of gold and silver nanoparticles and their potential application for cancer therapeutics. Materials Science and Engineering C 53, 298-309.

Pechyen, C., Ponsanti, K., Tangnorawich, B., Ngernyuang, N., 2021. Waste fruit peel-mediated green synthesis of biocompatible gold nanoparticles. Journal of Materials Research and Technology 14, 2982-2991.

Quiterio-Gutiérrez, T., Ortega-Ortiz, H., Cadenas-Pliego, G., Hernández-Fuentes, A.D., Sandoval-Rangel, A., Benavides-Mendoza, A., Cabrera-de la Fuente, M., Juárez-Maldonado, A., 2019. The application of selenium and copper nanoparticles modifies the biochemical responses of tomato plants under stress by *Alternaria solani*. International Journal of Molecular Sciences 20, 1950.

Ruangpan, L., Tendencia, E.A., 2004. Bacterial isolation, identification and storage. Laboratory Manual of Standardized Methods for Antimicrobial Sensitivity Tests for Bacteria Isolated from Aquatic Animals and Environment, Southeast Asian Fisheries Development Center, pp. 3-11.

Saeed, M., Mukhtar, T., Rehman, M.A., 2019. Temporal fluctuations in the population of citrus nematode (*Tylenchulus semipenetrans*) in the Pothowar region of Pakistan. Pakistan Journal of Zoology 51, 2257-2263.

Satti, S.H., Raja, N.I., Ikram, M., Oraby, H.F., Mashwani, Z.U.R., Mohamed, A.H., Omar, A.A., 2022. Plant-based titanium dioxide nanoparticles trigger biochemical and proteome modifications in *Triticum aestivum* L. under biotic stress of *Puccinia striiformis*. Molecules 27, 4274.

Sengupta, S., Biswas, S., Pradhan, A., Bhattacharya, M., 2024. Brief review study on citrus fruits: Blessing of nature. International Journal of Biology, Pharmacy and Allied Sciences 12, 1-10.

Shahbaz, M., Akram, A., Raja, N.I., Mukhtar, T., Mehak, A., Fatima, N., Ajmal, M., Ali, K., Mustafa, N., Abasi, F., 2023. Antifungal activity of green synthesized selenium nanoparticles and their effect on physiological, biochemical, and antioxidant defense system of mango under mango malformation disease. PLoS ONE 18, e0274679.

Sharma, D., Kanchi, S., Bisetty, K., 2019. Biogenic synthesis of nanoparticles: A review. Arabian

Journal of Chemistry 12, 3576-3600.

Sultana, T., Javed, B., Raja, N.I., Mashwani, Z.U.R., 2021. Silver nanoparticles elicited physiological, biochemical, and antioxidant modifications in rice plants to control Aspergillus flavus. Green Processing and Synthesis 10, 314-324.

Tahir, Z.B., Atiq, M., Rajput, N.A., Akram, A., Arif, A.M., Iqbal, S., Ali, S., Nawaz, A., Usman, M., Husnain, A., 2023. Determination of biochemical base line of resistance against bacterial leaf spot of chilli after application of plant defense activators. Journal of Global Innovations in Agricultural Sciences 11, 61-67.

Tarfeen, N., Nisa, Q., Kahlief, K., 2022. Antioxidant defense system in plants against biotic stress. Antioxidant Defense in Plants: Molecular Basis of Regulation, 383-395.

Ullah, H., Wilfred, C.D., Shaharun, M.S., 2019. Green synthesis of copper nanoparticle using ionic liquid-based extraction from *Polygonum minus* and their applications. Environmental Technology 40, 3705-3712.

Ullah, I., Ullah, A., Al-Qaaneh, A.M., Aman, K., Bekhit, M.M., Ullah, I., Farid, A., 2024. Green synthesis of silver and copper nanoparticles using *Parthenium hysterophorus*: Antibacterial, antioxidant, and anticancer properties. ChemistrySelect 9, e202401573.

Umair Raza, M., Abasi, F., Shahbaz, M., Ehsan, M., Seerat, W., Akram, A., Proćków, J., 2023. Phytomediated silver nanoparticles (AgNPs) embellish antioxidant defense system, ameliorating HLB-diseased 'Kinnow' mandarin plants. Molecules 28, 2044.

Villamizar, S., Ferro, J.A., Caicedo, J.C., Alves, L.M.C., 2020. Bactericidal effect of entomopathogenic bacterium *Pseudomonas entomophila* for *Xanthomonas citri* reduces citrus canker disease severity. Frontiers in Microbiology 11, 517533.

Wohlmuth, J., Tekielska, D., Hakalová, E., Čechová, J., Bytešníková, Z., Richtera, L., Baránek, M., 2024. Eliminating the pathogen *Xanthomonas hortorum* pv. *carotae* from carrot seeds using different types of nanoparticles. Agriculture 14, 498.